COMMUNICATION

A Generalizable Strategy for the 3D Bioprinting of Hydrogels from Nonviscous Photo-crosslinkable Inks

*Liliang Ouyang, Christopher B. Highley, Wei Sun, and Jason A. Burdick**

The three-dimensional (3D) manipulation of biofunctional components (e.g., cells, extracellular matrix, and growth factors) into tissue-like constructs is needed for tissue engineering and drug testing. Additive manufacturing approaches, such as 3D bioprinting, have attracted great interest for the deposition of materials (i.e., bioinks) and cells to build tissue structures, as they allow for application- and patient-specific designs at high resolution and enable structural complexity.[1,2] For most 3D bioprinting approaches (e.g., extrusion-based), a bioink needs to be extruded and then rapidly stabilized to maintain a printed structure, which is generally accomplished with bioinks that are highly viscous and/or that transition into solids through some external cue (e.g., ions, temperature).[3,4] Despite advances in bioinks, viscous bioinks can induce shear forces on cells during printing and compromise viability, and bioink design criteria toward printability severely limit material options. Thus, the balance between physical printability and biological functionality still remains a challenge for 3D bioprinting.[5,6]

Due to their varied material properties and ability to encapsulate cells, photo-crosslinkable hydrogels have great potential as bioinks.[7,8] However, despite the plethora of photo-crosslinkable hydrogels under development in the biomaterials field, their application to bioprinting is hindered through their generally low initial viscosity and challenges in polymerizing fast enough to maintain printed structures.[7] To overcome this limitation, photo-crosslinkable hydrogels have been combined with polymers that increase the precursor viscosity or that gel through other mechanisms, such as with temperature or ions.[9,10] This is not ideal, as it alters the material environment for cells and may need removal later. To directly print photo-crosslinkable materials, investigators have either pre-crosslinked or post-crosslinked the hydrogel to either increase the material viscosity prior to extrusion or rapidly cure the bioink after extrusion, respectively[10,11] (**Figure 1**A).

We illustrate the challenges with these approaches with methacrylated hyaluronic acid (MeHA) (Figure S1A, Supporting Information), a common photo-crosslinkable hydrogel that cures rapidly with light exposure (0.05 wt% I2959 photoinitiator, 5 wt% MeHA, Figure 1B) to form hydrogels of interest in applications ranging from cartilage tissue engineering[12] to the expansion of embryonic stem cells.[13] Pre-crosslinking (applying 10 mW cm^{-2} UV-irradiation for 30 s before extrusion) resulted in high and inconsistent extrusion forces (Figure 1C), heterogeneous printed material structures (Figure 1D and Movie S1, Supporting Information), and low cell viabilty (≈47%, Figure 1E). Shorter UV-irradiation times of 10 and 20 s improved cell viability, but still led to heterogeneous printed structures (Figure S2, Supporting Information). Post-crosslinking with light exposure after extrusion of the material improved cell viability and lowered the extrusion force; however, the bioink flowed prior to stabilization (Figure 1D and Movie S1, Supporting Information). In a previous study,[14] post-crosslinking was performed with a higher MeHA concentration of up to 20 wt% and higher UV intensity (15 mW cm^{-2}) and the bioink was still unable to maintain the filament structure.

To address these challenges in printing photo-crosslinkable materials, here we present a generalizable bioprinting method to enable 3D printing of hydrogel structures from photo-crosslinkable precursors. In this approach, we introduce the light through a photopermeable capillary (e.g., silicone tubing, glass) to crosslink the hydrogel immediately prior to deposition (Figure 1A and Figure S3A, Supporting Information), which we termed "in situ- crosslinking". Using MeHA, the forces for extrusion were low and consistent (Figure 1C), the printed filament was uniform (Figure 1D and Movie S1, Supporting Information), and high encapsulated cell viability (≈95%, Figure 1E) was possible. Advantages to this approach are: i) that it does not include any viscosity modulation or copolymerization with other polymers, ii) that it can be generalized to different photo-crosslinkable hydrogel formulations, iii) that it permits the encapsulation of viable cells, and iv) that it can be used to print heterogeneous and complex structures.

To develop this approach, we began by investigating the generation of the basic 3D building block in extrusion printing, the filament. To obtain continuous filaments, there should be minimal resistance between the filament and photopermeable capillary during crosslinking. When using a glass capillary, the extrusion force increased with time and, ultimately, the filament blocked the capillary (Figure S4, Supporting Information); however, treatment for hydrophobic modification resolved this and a consistent force and resulting filament was obtained (Figure S4, Supporting Information). When exploring additional capillary options, we found that commercial hydrophobic silicone tubing resulted in low and constant forces as well as the consistent formation of uniform filaments (Figure 1C and Figure S5, Supporting Information); thus, this tubing was used for subsequent studies.

Photo-crosslinking parameters are important to this in situ crosslinking approach, where the extent of photo-crosslinking

L. Ouyang, Dr. C. B. Highley, Prof. J. A. Burdick
Department of Bioengineering
University of Pennsylvania
210 South 33rd Street, Philadelphia, PA 19104, USA
E-mail: burdick2@seas.upenn.edu
L. Ouyang, Prof. W. Sun
Department of Mechanical Engineering
Tsinghua University
Beijing 100084, China

DOI: 10.1002/adma.201604983

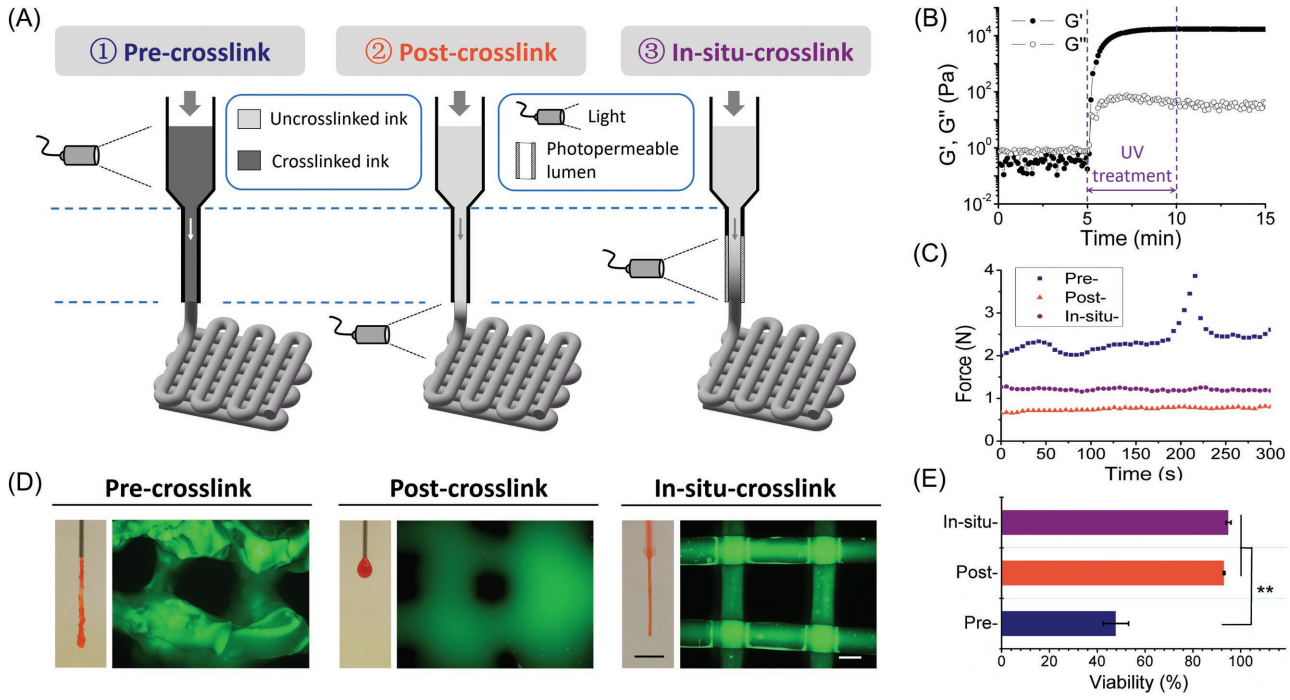

Figure 1. General bioprinting approach. A) Schematic of three different crosslinking strategies for bioprinting photo-crosslinkable inks (e.g., 5 wt% MeHA shown here), where crosslinking occurs before (pre-crosslink), after (post-crosslink), or during (in situ crosslink) extrusion. The in situ crosslinking process involves light exposure through a photopermeable capillary, during continuous extrusion, prior to deposition. B) Representative curves of storage (G') and loss (G'') moduli during irradiation of 5 wt% MeHA with UV light (10 mW cm^{-2}). C) Driving force consistency, D) representative images of nozzles with extruded material and printed lattice structure, and E) cell viability post printing for these three crosslinking strategies. In the pre-crosslink approach, the bioink was treated with 10 mW cm^{-2} UV light for 30 s before printing. In the post-crosslink and in situ crosslink groups, 10 mW cm^{-2} UV light was used. Scale bars: D, left) 5 mm, and D, right) 500 µm.

is controlled by the light intensity and exposure time for a given ink formulation (Figure S6A, Supporting Information) and the polymerization time is a function of both the length of the capillary that is exposed to light and the average velocity of the ink within the capillary. Using a capillary length of 30 mm and ink extrusion flux of 0.4 mL h^{-1}, low UV intensity (1 or 5 mW cm^{-2}) was insufficient to stabilize the filaments (Figure S7A, Supporting Information); however, increased light intensity (10 and 20 mW cm^{-2}) generated regular filaments. Filaments generated with 20 mW cm^{-2} had slightly larger diameters than those with 10 mW cm^{-2}, reflecting the extent of crosslinking; yet, consistent extrusion forces were measured for all intensities explored (Figure S7B, Supporting Information). To illustrate the influence of light intensity on the stability of printed structures, lattices were printed under different UV intensities, followed by poststabilization with added initiator and UV irradiation (≈2 min).[14] Low intensity (5 mW cm^{-2}) resulted in incomplete polymerization, while high intensity (>20 mW cm^{-2}) resulted in fiber separation when immersed in buffer (Figure S6C, Supporting Information) since there were not enough reactive groups remaining to crosslink printed fibers together. However, there was a window of light intensity (10 and 15 mW cm^{-2}) that resulted in stable structures (Figure S6C, Supporting Information). Thus, the extent of polymerization within the capillary is highly tunable and can be controlled for this process.

As the printed filaments are already crosslinked during deposition with this approach, it is necessary to control both the velocity of the extruded filament (the average velocity of the bioink in the capillary, v_{ink}) and the movement velocity of the nozzle during printing (v_{noz}). As illustrated in **Figure 2**A, these velocities should be matched to obtain a desired printed pattern when printing on a flat surface; when v_{ink} was lower or higher than v_{noz}, shorter or longer filaments than designed were generated, respectively, due to either pulling or compressive forces with deposition. When v_{ink} was equal to v_{noz}, MeHA filaments could be deposited in designed paths to build up structures (Movie S2, Supporting Information), including a lattice (Figure 2C), a tube structure 10 mm in diameter (Figure 2D), and a macroscale nose-shaped construct ≈10 mm in height (Figure 2E). Alternately, a hollow tube was printed by extruding the filament on a rotating rod, while the printer head moved along the length of the rod (Figure 2B and Movie S3, Supporting Information). By choosing suitable velocities of the extruded filament (v_{ink}) and nozzle movement during printing (v_{noz}), hollow tubes were obtained with diameters dependent on the diameter of the rod (Figure 2B).

Cohesion between layers of deposited filaments and structural stability were evident through the addition of water in the lumen of the printed tube structure (Movie S2, Supporting Information), where the tube maintained its integrity without leakage of water and could be manually manipulated (Figure 2F). Additionally, poststabilization enhanced the stability of the printed nose structure, which was maintained for up to one month (Figure S8, Supporting Information).

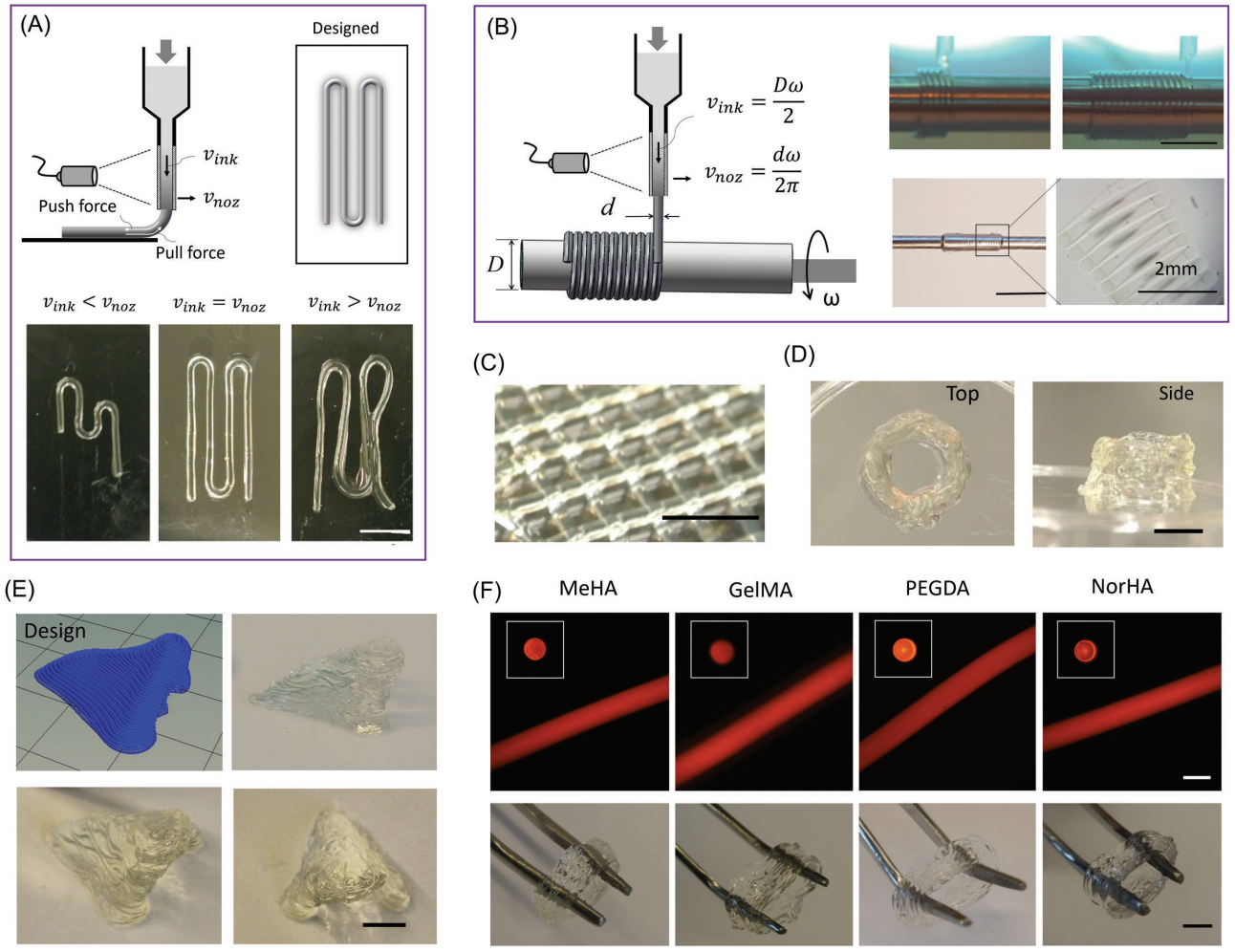

Figure 2. 3D printing photo-crosslinkable bioinks using the in situ crosslinking process. A) Schematic of filament deposition (top) with the ink velocity (v_{ink}) in the photopermeable capillary and nozzle moving velocity (v_{noz}) indicated; (bottom) images of printed filament based on a four-line model under different velocity configurations. B) Schematic of hollow tube printing on a rotating rod with the ink velocity (v_{ink}) in the photopermeable capillary and nozzle movement along the rod (v_{noz}) indicated, where D is the diameter of rotor, d is the diameter of the filament, ω is the angular velocity of the rotor; (top) representative images of printing process, showing the fabrication of a tube with diameter of ≈5 mm; (bottom) representative images of a printed tube with diameter of ≈1.5 mm on the rotor (left) and in buffer after removal from the rod (right). C–E) Representative images of printed lattice structure (C), hollow tube structure (D), and nose structure (E). In (A,C–E) 5 wt% MeHA was used and in (B) 2.5 wt% MeHA was used. F) (Top) Fluorescence images of printed filaments (labeled with rhodamine) with cross-sections as insets and (bottom) images of printed hollow tube structures undergoing stretching, printed using 2.5 wt% MeHA, 5 wt% GelMA, 5 wt% PEGDA, and 2 wt% NorHA bioinks. The applied UV intensity was 10 mW cm^{-2} for all bioinks. Scale bars: A–E) 5 mm unless otherwise stated, and F) 500 µm (top) and 5 mm (bottom).

Furthermore, the geometry of the printed filament was defined by the inner geometry and size of the capillary, leading to cylindrical shapes and diameters from 60 to 700 µm, which indicates high printing resolution with this approach (Figure S7C,D, Supporting Information).

To assess the cytocompatibility of the in situ crosslinking process, fibroblasts were encapsulated in a 5 wt% MeHA ink. High viability (≈95%) was observed after printing (**Figure 3**A) and no changes in cell density or viability were observed in filaments at different time points during a 40 min print period (Figure S9A–C, Supporting Information). Furthermore, cells printed into filaments with different sizes (≈200–700 µm) all maintained high viability (≈95%, Figure S9D,E, Supporting Information). High cell viability was maintained in a printed lattice and nose structure, with ≈90% viable cells observed (Figure S9F,G, Supporting Information). We attribute this high cell viability to the initially low viscosity of the bioink as the material and cells enter the capillary and the rapid and cytocompatible gelation that occurs within the capillary, which may protect cells from high shear stress. With extrusion and crosslinking occurring simultaneously, this process is quite different from a cellular perspective when compared to pre-crosslinking and postc-rosslinking approaches.

One of the major advantages to this in situ crosslinking approach is that it is generalizable to a range of photo-crosslinkable hydrogels. To illustrate this, we printed photo-crosslinkable gelatin methacryloyl (GelMA, ≈50% modification, Figure S10B, Supporting Information) and commercially available poly(ethylene glycol) diacrylate (PEGDA),[15,16] which undergo chain-growth polymerizations

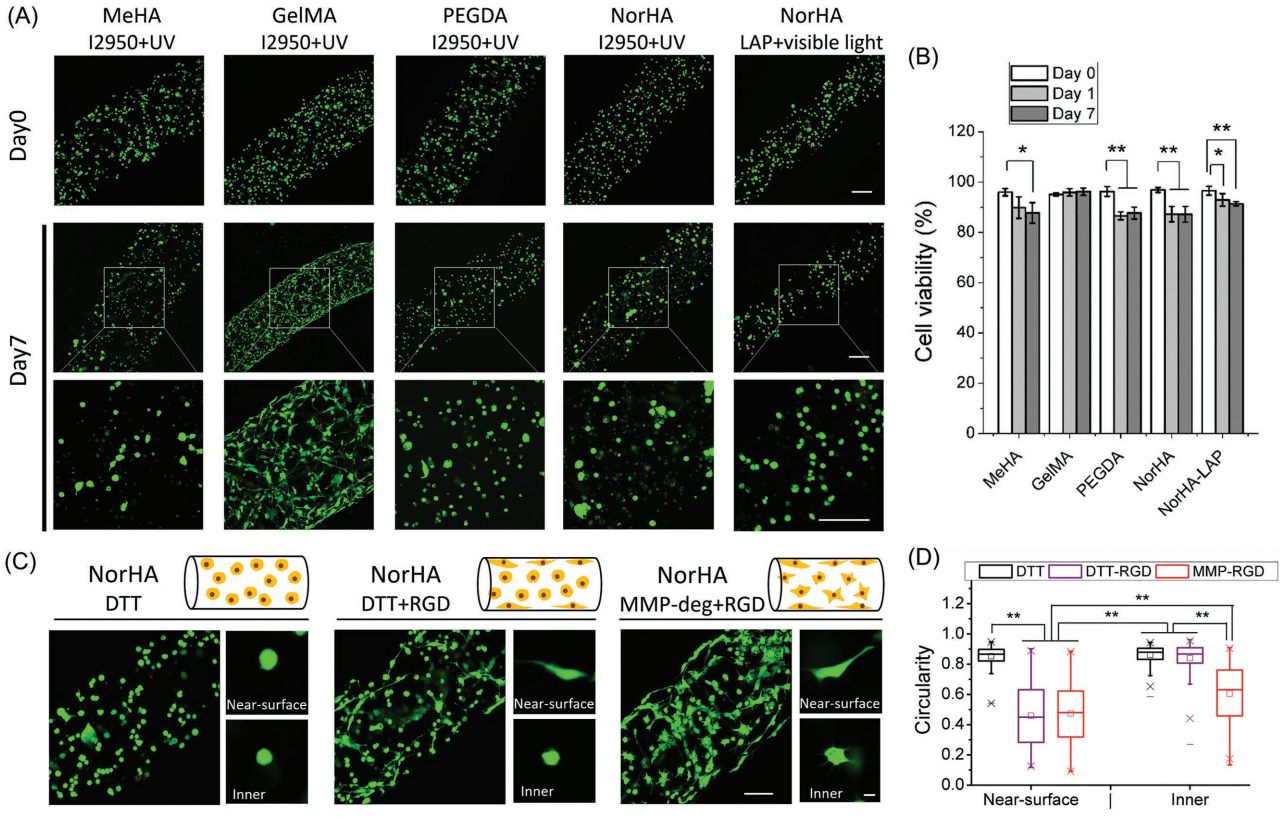

Figure 3. Viability and behavior of cells in bioprinted filaments. A) Fluorescence images of live/dead staining of 3T3 cells in printed filaments for different ink formulations as indicated at day 0 (postprinting) and at day 7. B) Quantified cell viability immediately postprinting and after 1 and 7 d in culture for different ink formulations. C) Magnified fluorescence images and representative single cell images at near-surface or inner core for three different formulations of NorHA bioink, either with or without RGD and using a nondegradable (DTT) or MMP-degradable crosslinker. D) Quantified cell circularity for cells at inner filament and surface locations for NorHA formulations. The applied UV and visible-light intensities were 10 and 15 mW cm^{-2}, respectively. Scale bars are: A) 200 µm and C) 100 µm and 10 µm (single cell images).

for gelation in the presence of light (Figure S1B,C, Supporting Information). We also explored thiol-ene reactions, which can overcome some of the oxygen inhibition of radical polymerizations[7] and undergo controlled crosslinking through reaction of a dithiol and an –ene (e.g., norbornene) in the presence of an initiator[17,18] (Figure S1D, Supporting Information). Specifically, norbornene-functionalized HA (NorHA) with ≈22% modification was synthesized and used as an ink (Figure S10C,D, Supporting Information). Bioinks from these precursors were formulated at low concentrations: 2.5 wt% MeHA, 5 wt% GelMA, 5 wt% PEGDA, and 2 wt% NorHA and low initial viscosities of 2.5–15 mPa s (Table S1, Supporting Information). Upon UV irradiation (10 mW cm^{-2}), a plateau for G' of 3–4 kPa for all groups was reached within minutes (Figure S11A–D, Supporting Information). Force measurements were confirmed to be consistent for all four formulations with magnitudes ranging from 0.8 to 1.5 N (Figure S12, Supporting Information) and all formulations were printed into regular filaments with standard circular cross-sections and built into extensible tube structures (Figure 2F).

This method represents a significant change from current extrusion-based bioprinting processes used in conjunction with photo-crosslinkable hydrogels that generally depend on initial viscosity modulation or copolymerization to establish printed structures. In the few reports on bioprinting photo-crosslinkable HA-based hydrogels, MeHA was primarily used and was often mixed with other components to enhance the printability, including examples with GelMA,[11,19] with thermoresponsive poly(*N*-isopropylacrylamide),[9] and as a further-modified guest–host shear-thinning formulation.[14,20] Here, inks could be printed as long as they could be sufficiently polymerized, which was based on MeHA concentration and light intensity (Figure S6, Supporting Information). GelMA has been more widely used and can be printed alone, but normally with 10 wt% or higher concentration for viscosity modulation[21–23] or with more than 7 wt% in noncontinuous approaches.[24] PEG-based photo-crosslinkable bioinks have been developed but rely on thermosensitive modifications,[15] copolymer formulations,[10] or pre-crosslinking[16] for bioprinting. Again, all of these approaches couple the final hydrogel properties with the ability to print, rather than toward controlling the environment surrounding the encapsulated cells.

The cytocompatibility of this general method was confirmed across diverse bioink formulations immediately and after one-week of culture, including with another group of NorHA crosslinked with the photoinitiator lithium phenyl-2,4,6-trimethylbenzoylphosphinate (LAP, 0.05%) and visible light (15 mW cm^{-2}) (Figure 3A). For all five formulations—MeHA,

GelMA, PEGDA, NorHA, and NorHA (LAP + Visible)—cells maintained high viability (≈96%) after printing (day 0) without significant differences across groups (Figure 3B). After one and seven days in culture, cell viabilities remained high (> 87%) across all groups. Cells in GelMA filaments were viable (≈95%) in one-week cultures and displayed spread and connected morphologies at day 7 compared with the other four groups, where cells were round and isolated within the hydrogel matrices (Figure 3A). This is likely attributed to the arginine–glycine–aspartic acid (RGD) sequences within gelatin for adhesion as well as sequences that are degradable in the presence of proteases (Figure S1B, Supporting Information).

This observation highlights a strength to this printing approach, where varied material properties that affect cell behavior can be introduced without concern of material printability. To illustrate this, we applied nondegradable dithiothreitol (DTT) or matrix metalloproteinase-degradable (MMP-deg) crosslinkers either with or without RGD functionalization to the crosslinking of NorHA hydrogels (Figure S1E and Table S1, Supporting Information). As shown in Figure 3C, when using a DTT crosslinker without RGD, cells in filaments were rounded both near the surface and within inner core areas at day 7; however, the addition of RGD led to cell spreading at the filament surface. When an MMP-degradable crosslinker and RGD were both used, cell spreading occurred not only at the surface but also within the filament. Single cell morphology "near the surface" and "inner" regions were quantified and supported these observations (Figure 3D). A confocal z-stack clearly showed the cell morphology changing throughout the regions in the various filaments investigated (Movie S4, Supporting Information). These data demonstrate the ability to tune cell behavior by modulating the bioink formulations with this in situ crosslinking approach.

Beyond the printing of simple filaments from a range of materials and with viable cells, another advantage of this method is the printing of complex heterogeneous filaments, such as with a coaxial nozzle (Figure S3B, Supporting Information). Through separation of different bioinks in the core and shell needles during printing, it was possible to generate core–shell filaments from multiple inks without or with cells (**Figure 4**A–C and Figure S13A, Supporting Information). Though core–shell filament-based constructs have been printed with alginate, collagen, and poly(ε-caprolactone),[25,26] photo-crosslinkable hydrogels were seldom applied directly. Furthermore, by controlling the on/off status of core and shell channels, heterogeneous filaments were printed with a programmable distribution of multiple inks or cell types along their length (Figure 4D–F and Figure S13B, Supporting Information), which has only been possible previously with microfluidic printheads.[27] Such multimaterial filaments are useful in building complex structures, which is now possible with photo-crosslinkable bioinks. As a last example, open-channel hydrogel tubes were printed using a coaxial nozzle with a longer core needle (Figure S3C, Supporting Information), so that irradiation of the shell occurred prior to the introduction of core material (Figure 4G and Figure S3D, Supporting Information). This produced hollow

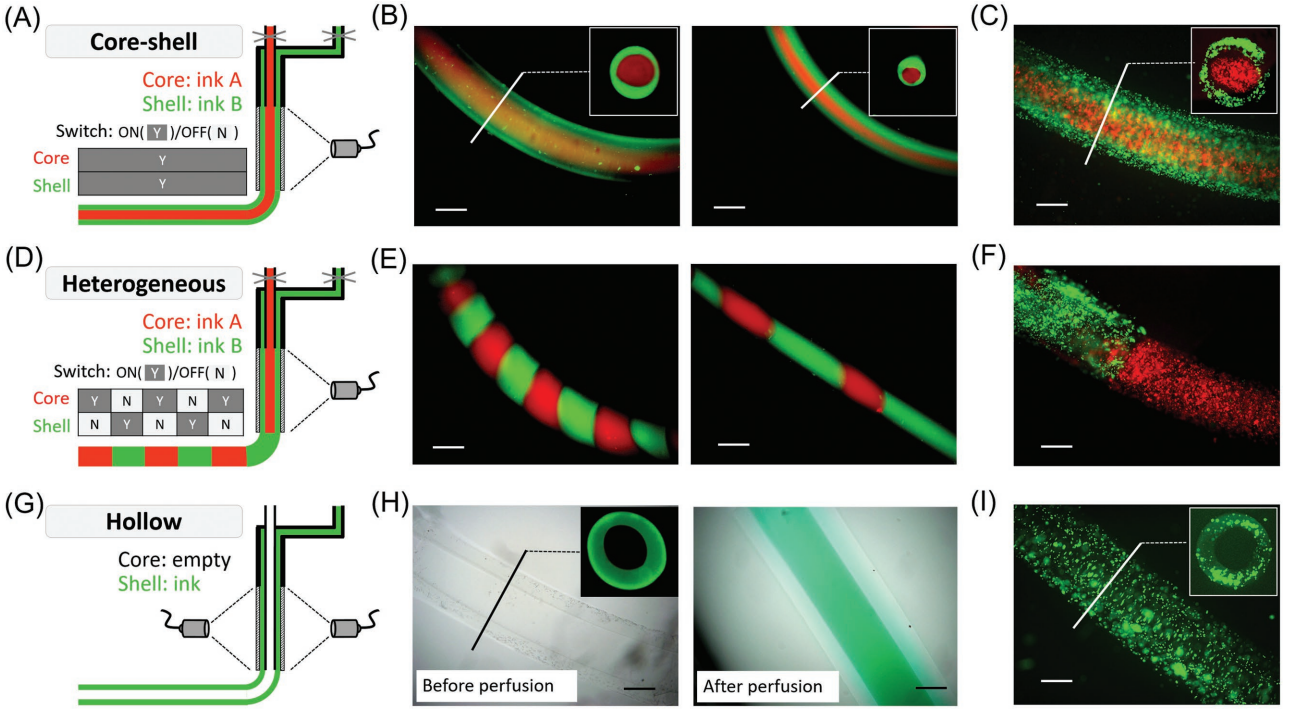

Figure 4. Complex printed structures with in situ crosslinking approach. A) Schematic and representative fluorescence images for printing filaments with core–shell structure using two inks labeled with different fluorophores (B) or two inks containing cells labeled with different dyes (C). D) Schematic and representative fluorescence images for printing heterogeneous filaments with intermittent structures using two inks labeled with different fluorophores (E) or two inks containing cells labeled with different dyes (F). G) Schematic for printing hollow filaments using a longer core coaxial nozzle and representative images of printed hollow tubes either before or after perfusion with a dye solution (H) or with cells in the printed tubes (I). The inset images are the cross-sections of core–shell (B,C) and hollow (H,I) filaments. Scale bars are 500 µm.

(cell-laden) filaments (Figure 4G–I and Figure S13C, Supporting Information) that could be perfused (Movie S5, Supporting Information). Although perfusable conduits of alginate have been reported,[28,29] our approach again makes this possible with a wide range of materials.

In conclusion, we developed a generalizable technology for 3D bioprinting of photo-crosslinkable hydrogels without limitations of ink viscosity. This was possible with introduction of a photopermeable capillary to simultaneously crosslink the bioink as it was being extruded. The printing of 3D structures (e.g., lattices, hollow tubes, and macroscale tissue constructs) was possible with a range of synthetic (PEGDA) and natural (MeHA, NorHA, and GelMA) bioinks and with both ultraviolet and visible light. All of these hydrogels were printed with consistent filaments and high cell viability (>90%), and the ability to tune cell behavior was demonstrated using thiol-ene crosslinkable NorHA in conjunction with RGD and degradable crosslinkers. Through use of a coaxial nozzle, this method was also used to print controlled, heterogeneous filaments that consisted of core–shell structures, hollow tubes, and heterogeneous material compositions along the filament length. This in situ crosslinking method advances our ability to print a wide variety of photo-crosslinkable hydrogels for biomedical applications.

Experimental Section

Material Synthesis and Bioink Formulation: HA- and gelatin-derived materials were synthesized as previously described[13,17,30] and as outlined in more detail in the Methods Section (Supporting Information). MeHA, NorHA, GelMA, and PEGDA raw materials were sterilized with 45 min UV irradiation before dissolving in sterile solutions of photoinitiator (0.05 wt% I2959 or LAP) and phosphate buffered saline (PBS). For NorHA, the crosslinker (DTT or MMP-deg) was calculated to consume 60% of norbornene groups with the optional addition of 3×10^{-3} M RGD. 3T3 fibroblasts were added when desired at a final cell density of 2.5×10^6 mL^{-1}, unless otherwise stated.

Bioprinter Setup: The 3D printer used was a fused deposition modeling (FDM) desk-top printer previously modified to print hydrogels.[20] Repetier software was used to slice computer-aided design (CAD) models and control the printing process. A spot cure lamp system (UV light: OmniCure S1000, 320–390 nm, or visible light: OmniCure S1500, 400–500 nm) with a collimating lens was used to introduce light to the photopermeable capillary, which was either silicone tubing or glass. When using soft silicone tubing, a suitable rigid helical cover was introduced (Figure S3A, Supporting Information).

Bioprinting: After mixing, the bioink (including with cells) was loaded into a syringe with modified photopermeable capillary and the syringe was loaded onto the printhead. UV or visible light was initially adjusted to focus on the photopermeable capillary at the desired intensity. Photopermeable capillaries 30 mm in length and a printing flux of 0.4 mL h^{-1} were used, unless otherwise stated. Optionally, to enhance the structural stability, printed structures were immersed in 0.05% photoinitiator solution for additional light irradiation (1–2 min). After printing, cell-laden structures were immersed in growth medium and incubated at 37 °C. A force measurement system (FlexiForce, Tekscan) was used to assess the extrusion consistency by putting the force sensor between the syringe pump driver and syringe's plunger. The force output was captured for 5 min during continuous extrusion at the flow rate of 0.4 mL h^{-1}, unless otherwise stated.

Cell Cuture and Live/Dead Staining: 3T3 fibroblasts were cultured in growth medium (α-minimum essential medium, 10% fetal bovine serum (FBS), 1% L-glutamine, and 1% penicillin-streptomycin) and used at passage 10 or less. To conduct live/dead staining, the printed cell-laden hydrogel structures were immersed in calcein-AM/ethidium homodimer solution for 20 min. Fluorescence (Olympus BX51) and confocal (Zeiss) microscopy systems were used to image the stained cell-laden structures. Image-J was used to quantify the cell viability ($n = 3$) and single cell circularity ($n = 100$–200).

Coaxial System: Two coaxial nozzles were used in this study. One had the same length for core (23G) and shell (18G) needles, while the other one had 10 mm longer inner needle (24G) than shell needle (18G) (Figure S3B,C, Supporting Information). Two independent syringe pumps were used to control the extrusion of core/shell channels, with the flow rate of 0.1–0.4 mL h^{-1}. Printing was performed either without or with labeled cells included.

Statistical Analysis: All data are presented as mean ± standard deviation. Statistical significance was determined by analyiss of variance (ANOVA) with Tukey honest significant difference (HSD) post hoc as $*p < 0.05$, $**p < 0.01$, $***p < 0.001$.

Supporting Information

Supporting Information is available from the Wiley Online Library or from the author.

Acknowledgements

The authors thank Dr. K. H. Song for his help in material preparation. This work was financially supported by the China Scholarship Council (File: L. O. 201506210148) and the National Science Foundation Materials Research Science & Engineering Center at the University of Pennsylvania.

Received: September 15, 2016
Revised: October 27, 2016
Published online: December 16, 2016

[1] J. Groll, T. Boland, T. Blunk, J. A. Burdick, D. W. Cho, P. D. Dalton, B. Derby, G. Forgacs, Q. Li, V. A. Mironov, L. Moroni, M. Nakamura, W. Shu, S. Takeuchi, G. Vozzi, T. B. Woodfield, T. Xu, J. J. Yoo, J. Malda, *Biofabrication* **2016**, *8*, 013001.
[2] C. Mandrycky, Z. Wang, K. Kim, D. H. Kim, *Biotechnol. Adv.* **2016**, *34*, 422.
[3] C. Colosi, S. R. Shin, V. Manoharan, S. Massa, M. Costantini, A. Barbetta, M. R. Dokmeci, M. Dentini, A. Khademhosseini, *Adv. Mater.* **2016**, *28*, 677.
[4] I. T. Ozbolat, M. Hospodiuk, *Biomaterials* **2016**, *76*, 321.
[5] L. Ouyang, R. Yao, Y. Zhao, W. Sun, *Biofabrication* **2016**, *8*, 035020.
[6] L. Ouyang, R. Yao, S. Mao, X. Chen, J. Na, W. Sun, *Biofabrication* **2015**, *7*, 044101.
[7] R. F. Pereira, P. J. Bartolo, *J. Appl. Polym. Sci.* **2015**, *132*, 42458.
[8] S. R. Caliari, J. A. Burdick, *Nat. Methods* **2016**, *13*, 405.
[9] M. Kesti, M. Muller, J. Becher, M. Schnabelrauch, M. D'Este, D. Eglin, M. Zenobi-Wong, *Acta Biomater.* **2015**, *11*, 162.
[10] L. A. Hockaday, K. H. Kang, N. W. Colangelo, P. Y. Cheung, B. Duan, E. Malone, J. Wu, L. N. Girardi, L. J. Bonassar, H. Lipson, C. C. Chu, J. T. Butcher, *Biofabrication* **2012**, *4*, 035005.
[11] A. Skardal, J. Zhang, L. McCoard, X. Xu, S. Oottamasathien, G. D. Prestwich, *Tissue Eng., Part A* **2010**, *16*, 2675.
[12] L. Bian, M. Guvendiren, R. L. Mauck, J. A. Burdick, *Proc. Natl. Acad. Sci. USA* **2013**, *110*, 10117.
[13] S. Gerecht, J. A. Burdick, L. S. Ferreira, S. A. Townsend, R. Langer, G. Vunjak-Novakovic, *Proc. Natl. Acad. Sci. USA* **2007**, *104*, 11298.
[14] L. Ouyang, C. B. Highley, C. B. Rodell, W. Sun, J. A. Burdick, *ACS Biomater. Sci. Eng.* **2016**, *2*, 1743.

[15] R. Censi, W. Schuurman, J. Malda, G. di Dato, P. E. Burgisser, W. J. A. Dhert, C. F. van Nostrum, P. di Martino, T. Vermonden, W. E. Hennink, *Adv. Funct. Mater.* **2011**, *21*, 1833.
[16] A. L. Rutz, K. E. Hyland, A. E. Jakus, W. R. Burghardt, R. N. Shah, *Adv. Mater.* **2015**, *27*, 1607.
[17] W. M. Gramlich, I. L. Kim, J. A. Burdick, *Biomaterials* **2013**, *34*, 9803.
[18] J. C. Grim, I. A. Marozas, K. S. Anseth, *J. Controlled Release* **2015**, *219*, 95.
[19] B. Duan, E. Kapetanovic, L. A. Hockaday, J. T. Butcher, *Acta Biomater.* **2014**, *10*, 1836.
[20] C. B. Highley, C. B. Rodell, J. A. Burdick, *Adv. Mater.* **2015**, *27*, 5075.
[21] W. Schuurman, P. A. Levett, M. W. Pot, P. R. van Weeren, W. J. Dhert, D. W. Hutmacher, F. P. Melchels, T. J. Klein, J. Malda, *Macromol. Biosci.* **2013**, *13*, 551.
[22] T. Billiet, E. Gevaert, T. De Schryver, M. Cornelissen, P. Dubruel, *Biomaterials* **2014**, *35*, 49.
[23] R. Levato, J. Visser, J. A. Planell, E. Engel, J. Malda, M. A. Mateos-Timoneda, *Biofabrication* **2014**, *6*, 035020.
[24] L. E. Bertassoni, J. C. Cardoso, V. Manoharan, A. L. Cristino, N. S. Bhise, W. A. Araujo, P. Zorlutuna, N. E. Vrana, A. M. Ghaemmaghami, M. R. Dokmeci, A. Khademhosseini, *Biofabrication* **2014**, *6*, 024105.
[25] G. Kim, S. Ahn, Y. Kim, Y. Cho, W. Chun, *J. Mater. Chem.* **2011**, *21*, 6165.
[26] K. Lee, C. R. Seo, J. M. Ku, H. Lee, H. Yoon, J. Lee, W. Chun, K. W. Park, G. Kim, *RSC Adv.* **2015**, *5*, 29335.
[27] J. O. Hardin, T. J. Ober, A. D. Valentine, J. A. Lewis, *Adv. Mater.* **2015**, *27*, 3279.
[28] Q. Gao, Y. He, J. Z. Fu, A. Liu, L. Ma, *Biomaterials* **2015**, *61*, 203.
[29] Y. Zhang, Y. Yu, A. Akkouch, A. Dababneh, F. Dolati, I. T. Ozbolat, *Biomater. Sci.* **2015**, *3*, 134.
[30] A. I. Van Den Bulcke, B. Bogdanov, N. De Rooze, E. H. Schacht, M. Cornelissen, H. Berghmans, *Biomacromolecules* **2000**, *1*, 31.